A thermodynamically consistent phase diagram of a trimorphic pharmaceutical, l -tyrosine ethyl ester, based on limited experimental data

Ivo B. Rietveld, Alain Polian, Josep-Lluis Tamarit, Béatrice Nicolaï, Maria Barrio, Pol Lloveras, Jean-Paul Itié

Journal Name

ARTICLE

A thermodynamically consistent phase diagram of a trimorphic pharmaceutical, L-tyrosine ethyl ester, based on limited experimental data

Béatrice Nicolaï,[a,b] Maria Barrio,[c] Pol Lloveras,[c] Alain Polian,[d] Jean-Paul Itié,[e] Josep-Lluis Tamarit[c] and Ivo B. Rietveld*[b,f]

Crystalline polymorphs possess different physical properties and phase changes between those polymorphs may affect the properties of engineered materials such as drugs. This is very well illustrated by the large effort that is put into the capability to predict phase behavior of pharmaceuticals to avoid the unexpected appearance of different crystal forms. Much progress has been made, but one of the remaining challenges is (the accuracy in) the prediction of phase behaviour as a function of temperature. Obviously, predictions should at a certain point be verified against experimental data, however, it may not always be easy to elucidate the phase behavior of a given compound experimentally, because thermodynamically and kinetically controlled phenomena occur in a convoluted fashion in experimental data. The present paper discusses the trimorphism of L-tyrosine ethyl ester as an example case of how experimental data in combination with the thermodynamic tenets lead to a consistent phase diagram, which can be used as the basis for pharmaceutical formulations and for comparison with polymorph predictions by computer. The positions of the two-phase equilibria I-II, I-III, and I-L have been obtained experimentally. Using the Clapeyron equation and the alternation rule, it has been shown how the positions of the other equilibria II-L, III-L, and II-III can be deduced in combination with the stability rankings of the phases and the phase equilibria. The experimental data have been obtained by synchrotron X-ray diffraction, Raman spectroscopy, and thermal analysis as a function of pressure and temperature. Furthermore, laboratory X-ray diffraction as a function of temperature and differential scanning calorimetry have been used. At room temperature, form II is the most stable phase, which remains stable with increasing pressure, as it possesses the smallest specific volume. Form I becomes stable above 33 °C (306 K), but with increasing pressure it turns into form III. On thermodynamic grounds, form III is expected to have a stable domain at very low temperatures.

a. *Université Paris Sud, Faculté de Pharmacie, UMR8612 Institut Gallien, 5 rue Jean-Baptiste Clément, 92296 Châtenay-Malabry, France.*

b. *Faculté de Pharmacie, Université Paris Descartes, Université Sorbonne Paris Cité, 4 Avenue de l'Observatoire, 75006 Paris, France.*

c. *Grup de Caracterització de Materials, Departament de Física and Barcelona Research Center in Multiscale Science and Engineering, Universitat Politècnica de Catalunya, EEBE, Campus Diagonal-Besòs, Av. Eduard Maristany 10-14, 08019 Barcelona, Catalonia, Spain.*

d. *Sorbonne Université, CNRS UMR 7590, Institut de Minéralogie, de Physique des Matériaux et de Cosmochimie, 4 Place Jussieu, 75005 Paris, France.*

e. *Synchrotron SOLEIL, L'Orme des Merisiers Saint-Aubin, BP 48, 91192 Gif-sur-Yvette, France.*

f. *Normandie Université, Laboratoire SMS - EA 3233, Université de Rouen, 76821 Mont Saint Aignan, France.*

Introduction

Stability ranking of crystalline polymorphs

Phase behaviour is an important issue for materials that need to remain stable, such as active pharmaceutical ingredients and their drug formulations, explosives, and industrial installations that have to sustain large changes in temperature and or pressure.[1] In cases, where failure is not acceptable, the phase behaviour of the materials has to be studied, because different phases have different properties. It involves on the one hand the prediction of the possible phases that may exist,[2-4] and on the other hand, a ranking of those phases that are known to exist in the order of their relative stability as a function of the conditions that the system is submitted to.[5-9] Relative stability between different phases will indicate the possibility of phase change. Prediction of crystal structures in combination with their stability ranking is becoming a powerful method. However, the calculations have to be verified against experimental data to make sure that the approach is valid and this is not only true for the structural data[10] but also for the

stability data as a function of temperature and pressure.[11-13] It may be well known that adding temperature dependence to computer calculated stability rankings is difficult,[14] but it should not be forgotten that the experimental determination of equilibrium temperatures can be problematic too.[15]

Kinetics versus thermodynamics in an experiment

In the ideal case, one would like to map precisely the thermodynamics and kinetics of the phase behaviour of a given substance (or mixture of substances). Phase equilibria are generally studied by observing the related phase transitions.[16, 17] However, due to kinetics, certain phase transitions may be difficult to observe or the conditions of observation of the phase transitions are not the actual equilibrium conditions.[15, 18-23] A convenient example to illustrate this point is the solid-solid transition of L-tyrosine ethyl ester (L-TEE). At a scanning rate of 10 K min⁻¹ with a differential scanning calorimeter (DSC), the transition from solid form II to solid form I was observed around 65 °C (338 K).[23] Only by lowering the scanning rate of the DSC gradually, could it be observed that the transition temperature levelled off at around 33°C (306 K).[23] Moreover, once L-tyrosine ethyl ester had converted into form I, it did not revert back into form II. This was observed experimentally by lack of any transition in the DSC or X-ray from form I into form II at room temperature and by the fact that L-tyrosine ethyl ester is commercially available as pure form I.[23, 24] Such a finding may lead to the conclusion that form I is actually the stable form at room temperature, but the combination of two observations contradicts this. First of all form II can be kept at room temperature indefinitely, which became already clear during previous experiments[23] and which is confirmed by the synchrotron measurements presented below. The second observation is that exposure of L-TEE form II to temperatures above 33°C (306 K) would cause it to convert into form I. As conversion rates generally do not change from significant to negligible unless some sort of transition has taken place, lowering the temperature would for a metastable form II simply lower the conversion rate into form I and not eliminate the conversion. Therefore, it can be concluded that form II is the stable form at room temperature (no formation of form I observed at RT), form I is the stable form at 33°C (306 K) and higher temperatures (transition observed from form II into form I at 33°C) even if the transition rate of form II into form I is not fast (scanning by DSC at 10 K min⁻¹ tends to overshoot the transition temperature) and that the transition of form I into form II is kinetically inhibited (no transition of form I into form II observed at room temperature: commercial form is form I).[23] In conclusion, it is important that the thermodynamic description of the system is in accordance with all the experimental observations.

The system: L-tyrosine ethyl ester

The subject of this study, the aforementioned L-tyrosine ethyl ester is a prodrug for the delivery of the amino acid L-tyrosine in the human body. The esterification increases the
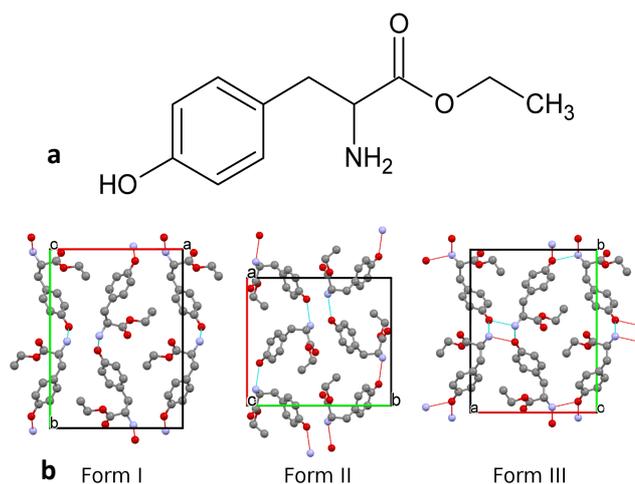
Figure 1. (a) L-tyrosine ethyl ester (209.24 g mol⁻¹). **(b)** The packing of the three polymorphs.[23,24,29]

lipophilicity of the amino acid improving absorption in the intestines.[25, 26] In addition, these short-chained esters tend to hydrolyse slowly reducing the rate of clearance in the liver and providing a gradual release of the amino acid in the body.[26-28] The molecule consists of a hydroxyl phenyl moiety linked through an additional carbon atom to the amino acid moiety and an ethyl ester group (see Figure 1). The ethyl ester tail exhibits two main conformations leading to crystalline trimorphism (Table 1).[29] The first structure, that of polymorph I, was first described in 1970 for the stereoisomer D-tyrosine ethyl ester (Cambridge Structural Database (CSD): TYREST)*.[30] Its crystal system is orthorhombic with space group $P2_12_12_1$, as is the case for the other two polymorphs. Its unit cell has a volume of 1146.4 Å³ at room temperature with $Z = 4$ (Table 1). More recently, from powder diffraction, the unit cell was found to be 1152.4 Å³.[24] The second polymorph, whose structure was obtained from powder diffraction has a slightly smaller unit-cell volume of 1106.0 Å³ at room temperature and $Z = 4$, however, the molecular conformation is clearly different from polymorph I (CSD: XAVVIB).[23] More recently and serendipitously, a third form was discovered while investigating the pressure-temperature phase diagram of the

---

*Even though TYREST represents the structure of D-TEE, which is the stereoisomer of L-TEE, their crystal system, space group, powder diffraction pattern and unit-cell volume are equivalent. A mathematical transformation of TYREST into its mirror image results in the crystal structure of L-TEE. The conformation of L-TEE form I in the graphical abstract has been obtained in this way.

two previously discovered polymorphs. Form III, a high-pressure form, whose structure was resolved from a high-pressure powder diffraction pattern, has a unit-cell volume of 1057.6 Å[3] at 323K and 600 MPa with Z = 4 (CSD: XAVVIB01). In this case the molecular conformation is very close to that of the first form; its identity as a separate polymorph is defined by a single additional hydrogen bond.[29] Thus, L-TEE exhibits conformational polymorphism[1, 5, 6, 31] and both conformations (polymorphs I and II) exist or persist under ambient conditions.[23]

Table 1. Crystallographic data at room temperature (except for polymorph III [a]) of the L-TEE polymorphs,[b] which all exhibit an orthorhombic crystal system, a P2₁2₁2₁ space group and Z = 4

Form	Unit cell parameters (Å)			V (Å³)	Density (g/cm³)	Ref
	a	b	c			
I	12.788(5)	16.982(5)	5.279(5)	1146.42	1.2123	30
II	12.8679(8)	14.7345(8)	5.8333(4)	1106.01	1.2566	23
III	12.655(4)[a]	16.058(4)[a]	5.2045(12)[a]	1057.6[a]	1.3141[a]	29

[a] at 580 MPa and 323 K; [b] CSD Refcodes: I TYREST (D-TEE see text), II XAVVIB, III XAVVIB01

Experimental construction of a pressure-temperature phase diagram

In the present paper it will be demonstrated how a complete topological phase diagram can be constructed using the trimorphism of L-TEE as an example. Topological in this context signifies a structural phase diagram in which the positions of the different phase domains relative to each other are provided. The accuracy of the coordinates of the involved phase equilibria depends on the quantity and quality of the data on which they are based and on the level of extrapolation that has been used to obtain the coordinates. The data have been obtained through DSC,[23] X-ray diffraction as a function of temperature,[23] high-pressure thermal analysis,[23] synchrotron diffraction as a function of pressure and temperature,[29] and Raman spectroscopy as a function of temperature and pressure. Only the solid-solid transitions between I and II and between I and III and the melting equilibrium of form I have been experimentally observed.[23, 29] The rest of the diagram has been obtained using thermodynamic relationships.

The Clapeyron equation

The three most important elements in the topological approach are the Clapeyron equation, the alternation rule, and the concept of "ordinary conditions". The Clapeyron equation is well known:

$$\frac{dP}{dT} = \frac{\Delta S}{\Delta V} = \frac{\Delta H}{T \Delta V} \tag{1}$$

It provides the slope of a phase equilibrium dP/dT if the differences in entropy, ΔS, and in volume, ΔV, between the two involved phases are known. The volume differences can be obtained through volumetric measurements or by X-ray diffraction preferably as a function of temperature.[32] The entropy difference can be obtained from thermal measurements, as the entropy is equal to the enthalpy difference between the phases, ΔH, divided by the equilibrium temperature, T, at which the enthalpy change has been obtained.

The alternation rule

Because triple points are intersections of three different two-phase equilibria, the triple points form the backbone of any (topological) phase diagram; once their positions are known, the phase equilibria can be traced as straight lines in a first approximation connecting the triple points. Stable two-phase equilibria intersecting a triple point will decrease in stability ranking, due to the fact that on the opposite site of the triple point it enters a domain, in which a third phase -not involved in the two-phase equilibrium- is the most stable phase. This is all related to the fact that a pressure-temperature phase diagram is nothing more than the projection on the pressure-temperature plane of the intersections of the Gibbs free energy surfaces of the different phases (see also Figure 2 in ref 9). As a result, around a stable triple point, one will always find alternatingly a stable and a metastable two-phase equilibrium (the alternation rule) as illustrated later on in this paper (see for example Figure 9 in the discussion of this paper). If the triple point itself is metastable, the stability ranking of the involved two-phase equilibria will be lowered accordingly resulting in alternating metastable and supermetastable two-phase equilibria around the metastable triple point (see for example the grey circles in Figure 11a).

"Ordinary conditions": dealing with real systems
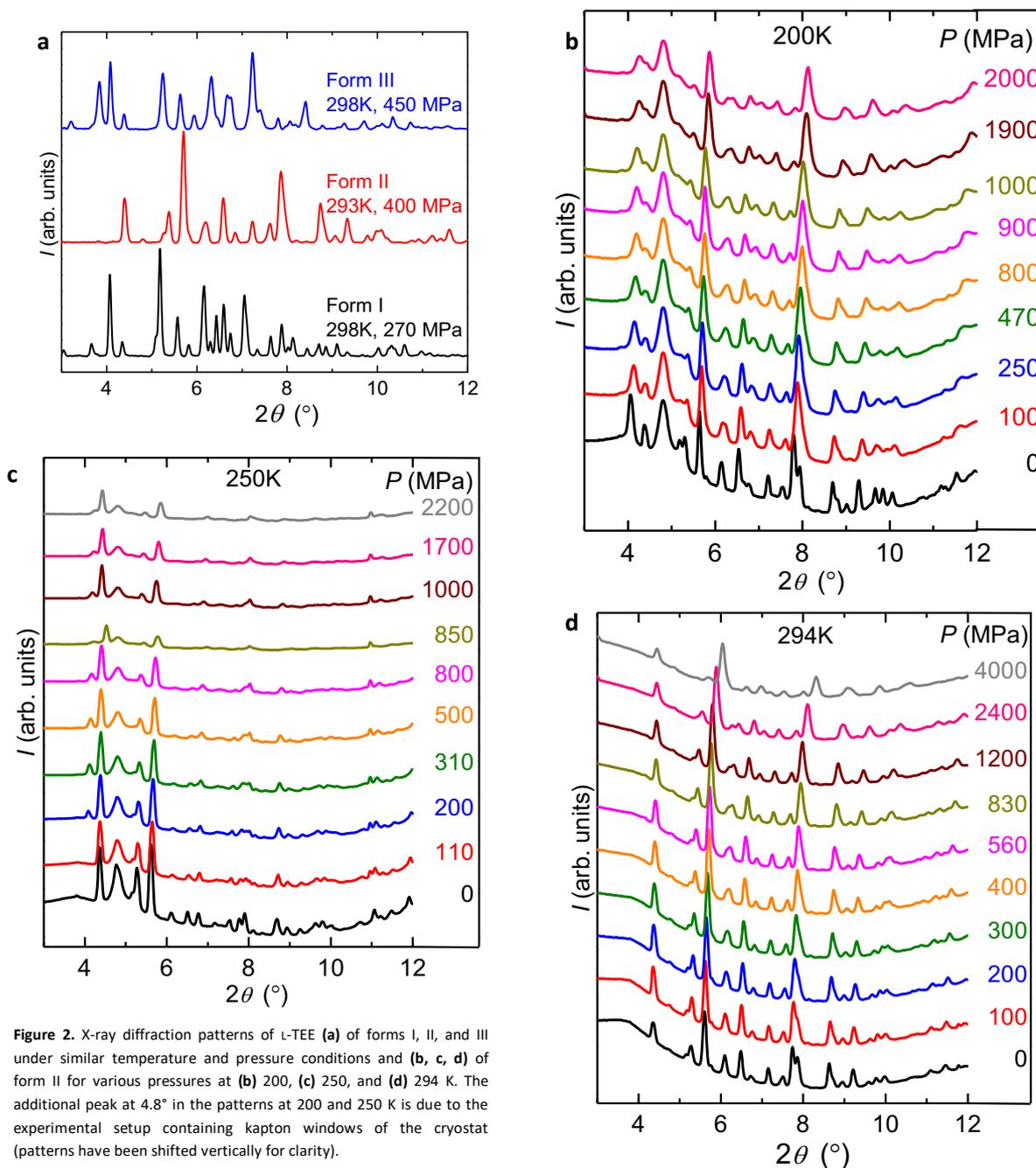
Figure 2. X-ray diffraction patterns of L-TEE **(a)** of forms I, II, and III under similar temperature and pressure conditions and **(b, c, d)** of form II for various pressures at **(b)** 200, **(c)** 250, and **(d)** 294 K. The additional peak at 4.8° in the patterns at 200 and 250 K is due to the experimental setup containing kapton windows of the cryostat (patterns have been shifted vertically for clarity).

The last important notion is that of "ordinary conditions". Thermodynamics deals with the equilibrium state; thus under a given pressure and temperature, it indicates which phase is the most stable. This may be a solid under pressure, an equilibrium between a solid and a liquid and so on; however, what happens to a solid substance in open air? As this substance is free to sublime, it is in principle not in equilibrium (it would be once it has filled the entire atmosphere with its vapour). However, we all know what happens to a sugar cube, salt, or even our desk out in the open. They remain intact, because practically, their vapour pressures are so low, that sublimation does not occur or is at least negligible on our timescale. Therefore the term "ordinary conditions" is used to indicate that the system under consideration is in thermal equilibrium with its surroundings and that it has basically saturated its close surroundings with its vapour phase, which is considered in equilibrium with the condensed phase. The term "ordinary conditions" also indicates that the thermodynamic pressure of the system is equivalent to its own (partial) vapour pressure. This can also be applied to substances in DSC pans and X-ray capillaries, which contain a finite space. Even if vapour pressures are low, the dead volumes in these containers can be considered occupied with the vapour phase that is practically in equilibrium with the solid or the liquid phase. It implies that measurements carried out with DSC pans and capillaries not subjected to any applied hydrostatic pressure practically follow the solid-vapour equilibrium line and after melting the liquid-vapour equilibrium line. This in

turn implies that melting points and solid-solid transitions obtained by DSC or X-ray diffraction are practically the same as triple points, because three phases are in equilibrium with each other: the vapour phase and two condensed phases. This approach is strictly speaking an approximation, but for substances with a low vapour pressure, in the order of a few pascals or less, the error is negligible.

Materials and Methods

L-Tyrosine ethyl ester

L-Tyrosine ethyl ester (M = 209.24 g mol^{-1}) was purchased from Sigma–Aldrich (Spain) (98%) and used as provided. Phase II was obtained as described in a previous paper by melting and recrystallization from the undercooled melt.[23] Phase III exists under pressure in samples that originally contained phase I.[29]

Diamond anvil cell

High pressure was generated with a membrane driven diamond anvil cell.[33] The anvil culet was 400 μm and the experimental volume drilled at the center of the imprint had a diameter of 200 μm. The gasket material was stainless steel in the case of the Raman experiments and CuBe for the synchrotron diffraction measurements. The pressure-transmitting medium was silicon oil and the pressure was measured using the linear ruby fluorescence scale.

Synchrotron X-ray diffraction

Diffraction data were collected at the high-pressure diffraction beamline PSICHE at the synchrotron SOLEIL (Gif sur Yvette, France). The diffraction data were obtained in two separate experiment runs with different wavelengths: 0.4499 and 0.4859 Å. The temperature was controlled with a liquid-nitrogen cryostat and an in-house constructed heater. Diffraction images were treated with the program fit2D.[34] Measurements have been carried out by varying the pressure at a set temperature (200K, 250 K, 294 K, 323K, and 337 K, and a few measurements at 303 K). The sample was allowed to

equilibrate before each measurement for about 15 minutes, which was extended to 1 hour at 200 and 250 K.

Pawley refinement has been carried out using TOPAS-Academic[35, 36] on all diffraction profiles of forms I, II, and III and the unit-cell volumes have been extracted and presented below as a function of pressure and temperature. The respective crystal structures can be found in previous publications.[23, 24, 29]

Raman spectroscopy

High-pressure, high-temperature Raman scattering experiments have been carried out in the backscattering geometry using a Jobin-Yvon HR-460 single monochromator spectrometer with a 1500 grooves/mm grating and a CCD camera as a detector. The 514.5 nm wavelength radiation from an Ar laser was focused into a 2 μm spot. Single crystals of L-TEE forms I and II were studied in separate experiments. Measurements were performed between 0 and 1.2 GPa and between 295 and 340 K. The spectra are limited to 1300 cm^{-1}, because of the strong first order Raman mode of the diamond anvils.

Results

Diffraction patterns of form II as a function of temperature and pressure

Synchrotron scattering data have been obtained as a function of temperature and pressure for form I and form II. The data of form I have been published previously together with the description of the structure of form III.[29] The diffraction data of form II are presented in Figure 2.

Specific volumes of forms I, II, and III as a function of pressure and temperature

From these data and those published previously, the unit cell volumes of forms I, II, and III have been determined as a function of pressure and temperature. The unit cell volume of form I is presented in Figure 3a. It can be seen that the dependence for form I in the pressure interval up to 400 MPa
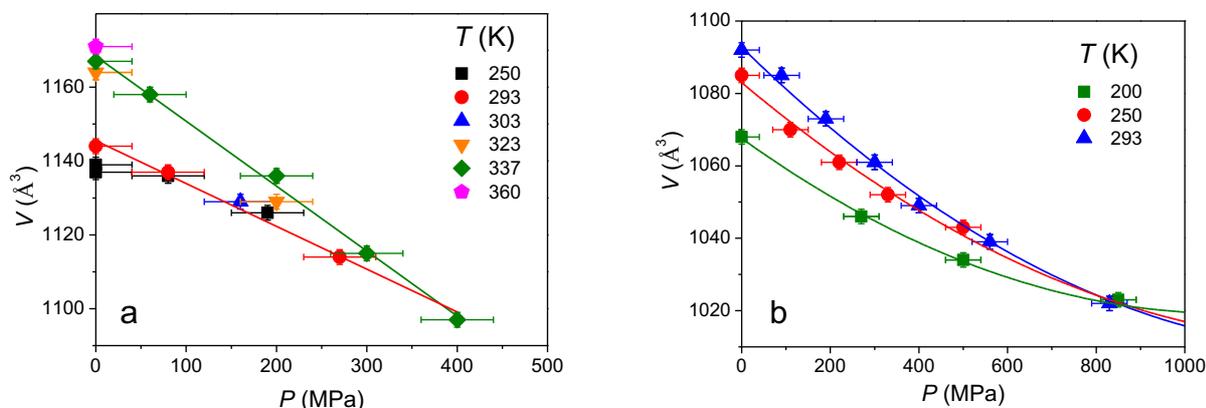
Figure 3. (a) The unit-cell volume of form I as a function of pressure at various temperatures. The volumes appear to converge at ~1100 Å^3 at a pressure of 400 MPa. **(b)** The unit-cell volume of form II as a function of pressure from 0 to 1000 MPa at 200, 250, and 293 K. In this case the volume converges around 850 MPa at 1020 Å^3.
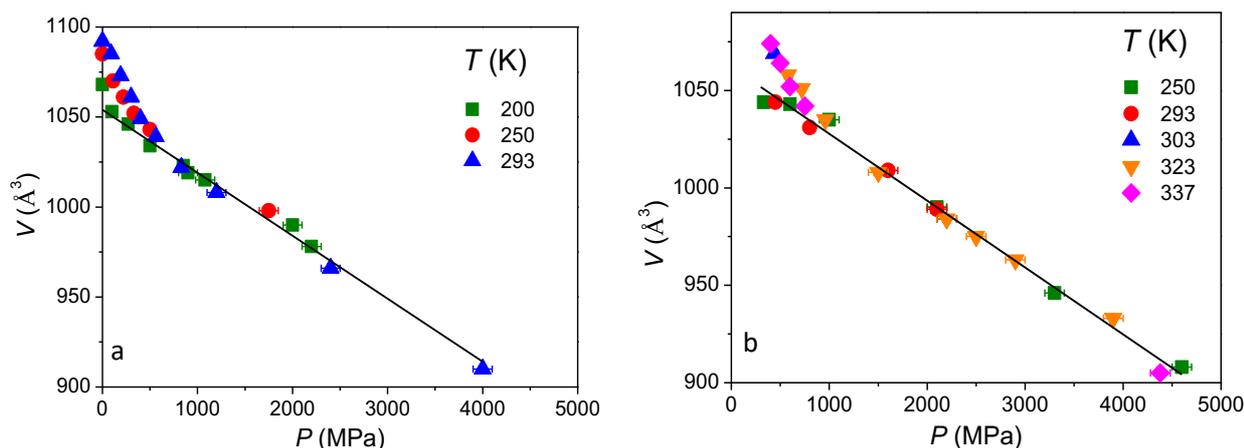
Figure 4. (a) The unit-cell volume of form II up to 4000 MPa in the temperature range of 200 to 293 K. **(b)** Unit-cell volumes of form III as a function of pressure at various temperatures.

is linear. Only for 293 K and 337 K, enough data exist to determine linear expressions leading to:

$$V_I (293\ K) = 1145.5(9) - 0.116(6)\ P \tag{2}$$
$$V_I (337\ K) = 1168.4(1.4) - 0.176(6)\ P \tag{3}$$

with V_I the unit cell volume of form I in Å³, and P the pressure in MPa.

The unit-cell volume of form II as a function of pressure and temperature is presented in Figure 3b for the pressure range 0 – 1000 MPa and up to 4000 MPa in Figure 4a. The dependency could only be measured up to 293 K, because just above this temperature form II turns into form I. It can be seen that the unit-cell volume is slightly curved with pressure, however, they become virtually the same at about 850 MPa irrespective of the temperature. The following quadratic curves describe the pressure behavior of the volume of form II between 0 and 850 MPa:

$$V_{II} (200\ K) = 1067.6(1.4) - 0.088(8)\ P + 4.0(8) \times 10^{-5}\ P^2 \tag{4}$$
$$V_{II} (250\ K) = 1083.0(1.6) - 0.103(9)\ P + 3.7(9) \times 10^{-5}\ P^2 \tag{5}$$
$$V_{II} (293\ K) = 1092.8(8) - 0.120(6)\ P + 4.3(6) \times 10^{-5}\ P^2 \tag{6}$$

Above 850 MPa, the unit cell data fall roughly on a single line for all different temperatures:

$$V_{II} (>850\ MPa) = 1053(3) - 0.0349(13)\ P \tag{7}$$

The data is not necessarily exactly the same for the different temperatures, but within the present experimental setting the variation is indistinguishable.

The unit-cell volumes of form III as a function of pressure and temperature are provided in Figures 4b and 5. At higher pressures, above 1000 MPa (Fig. 4b), all data appear to fall on a single line:

$$V_{III} (>1000\ MPa) = 1061(2) - 0.0339(7)\ P \tag{8}$$

Below this pressure, also 250 K and 293 K appear to lie on the line given by 8 and the data points for these two temperatures

have been used for the fit of expression 8 together with the data obtained above 1000 MPa. At 337 K and 323 K, there is enough data to observe a certain curvature, which has been fitted down from 1500 MPa, but it is hard to say with a lack of data between 1000 MPa and 1500 MPa, where the volume really significantly starts to deviate from the lower temperatures. In any case for 337 K and 323 K below 1500 MPa, the unit-cell volumes can be described by the expression:

$$V_{III} (323\text{-}337\ K) = 1104(8) - 0.091(2)\ P + 1.9(8) \times 10^{-5}\ P^2 \tag{9}$$

The volumes of form III and those of form II are very close; however, it is difficult to precisely compare their volumes, because the pressure and temperature ranges at which the volumes of the two forms have been obtained are different in particular at lower pressure. Where the temperatures are the same for 250 K and 293 K, the scatter over the data of form III is too large to draw any solid conclusions. This scatter in the data is the result of a slowing transition rate between I and III resulting in diffraction patterns containing two phases from which the unit-cell volumes are more difficult to obtain. However, at pressures above 1000 MPa, it can be seen that
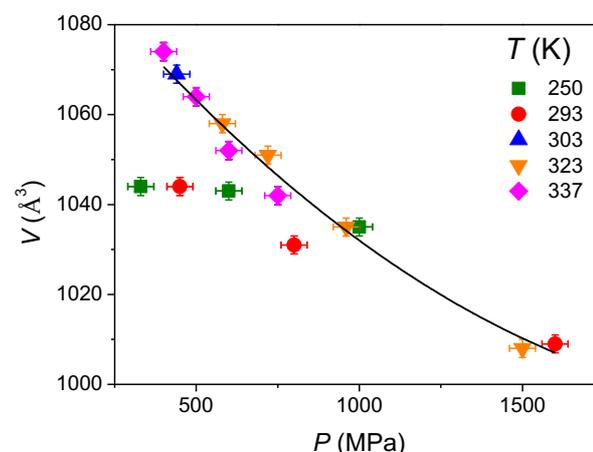
Figure 5. The unit-cell volumes of form III for 337K and 323K appear to be slightly curved towards higher values than at 293 and 250 K below 1500 MPa. There is too little data for 293 K to decide on any curvature in the pressure range 300-1000 MPa.

ARTICLE

form III has a slightly larger volume (eq. 8) than form II (eq. 7) and that this remains the case over the entire upper pressure range as the slopes are basically the same. This is an important thermodynamic result, as it means that the transition from form II into form III coincides with an increase in volume.

Birch-Murnaghan fits

The equations relating the unit-cell volume (or specific volume) directly with the pressure are convenient to interpret and construct the phase diagram discussed below, however these simple polynomials do not provide any information on the bulk modulus. The latter can be obtained with the Birch-Murnaghan expression of which the 4th order equation can be found in the supplementary information (SI. 21). Fits on the data have been carried out with the program EosFit7 by Angel et al.[37,38] The resulting values are compiled in Table 2: the unit-cell volume at zero pressure for a given temperature (V_{0T}), the bulk modulus at zero pressure for a given temperature (K_{0T}), its first derivative with respect to the pressure(K'_{0T}), and its second derivative with respect to the pressure (K''_{0T}).

Table 2. Birch-Murnaghan fit parameters (see SI. 21 for the 4th order equation) [a]

Form	T (K)	V_{0T} (Å³)	K_{0T} (GPa)	K'_{0T}	K''_{0T} (GPa⁻¹)
I	250	1138.5(1.4)	16(5)	[4]	
					[−0.25]
I	293	1145.3(1.4)	9.1(1.5)		
				[4]	[−0.43]
I	337	1167(2)	5.9(5)		
				[4]	[−0.66]
II	200	1066.9(2.1)	11.6(2.4)	26(10)	[−44]
II	250	1082(94)	9(62)	30(278)	[−82]
II	293	1091.9(1.4)	9(9)	11.7(2.0)	[−7.9]
III	323	1101(12)	12.5(4.1)	8.3(3.9)	[−2.2]
III	337	1118(13)	9.0(2.0)	[4]	[−0.43]

[a] Values between brackets are implicit and the result of truncating the 4th order equation to a lower order version depending on the available data.[37]

Plots of the parameters (V_{0T} and K_{0T}) obtained with the Birch-Murnaghan fit are provided in the supporting information (S7 and S8). It can be seen that the unit-cell volume of form I is significantly larger than those of forms II and III at zero pressure, whereas the volumes of forms II and III are very similar in accordance with the conclusions above. In the case of the bulk modulus, form II has the lowest bulk modulus, whereas form III seems to have the largest one for a given temperature, indicating that overall form III is the more rigid polymorph of the three.

Raman data of forms I, II and III as a function of temperature and pressure

Raman spectroscopy data of form I turning into form III as a function of pressure at 293 K are presented in Figure 6 and are used to complement[39] the X-ray data of forms I and III in which this transition had been observed (Table S2).[29] Observed wavenumbers of L-TEE (form I and II under ambient conditions) for the Raman data have been listed in Table S3 in the supplementary materials together with their assignments and comparison to a few other L-tyrosine esters.
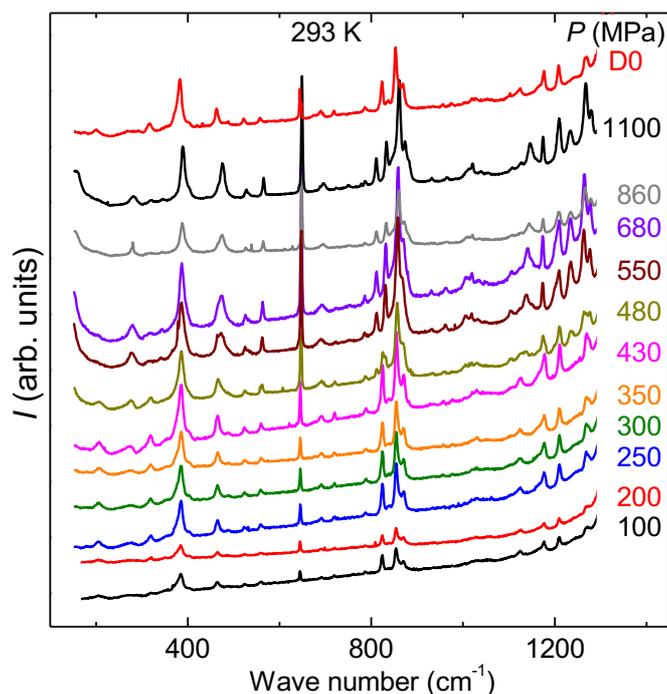

Figure 6. Raman spectra from 200 to 1300 cm⁻¹ at 293 K under pressure. Form I changes into form III between 430 and 480 MPa (see peaks at 200-300, 820-830, 1220 cm⁻¹), D: decompression. This figure is also provided in the supplementary materials (Figure S3) with data at 310 K (Fig S4), 320 K (Fig S5), and 340 K (Fig S6) in addition to ambient data for form II under pressure (Fig S2) and additional data of form I at ambient temperature (Fig S1).

Refining the position of the I-III equilibrium line with the Raman data

With the Raman data in Figure 6 (and Figures S1-S6 in the supplementary materials) and the synchrotron data as a function of temperature and pressure of forms I and III from a previous paper[29] a more precise estimate could be obtained for the position of the I-III equilibrium line than a former result based on X-ray diffraction data alone.[29] The observation of the appearance of form III with increasing pressure has been recorded in Figure 7 as well as the observation of the appearance of form I with decreasing pressure (see also Table S2). It can be seen that certain points almost overlap and that the hysteresis of the phase transition is very limited (the interval between the observation of form III and form I is mainly because it is very hard to control the pressure in the diamond anvil cell causing the pressure to change more than required for the phase change, while adjusting the pressure). Hysteresis does increase however at lower temperatures, because the phase transition becomes slower. To obtain an estimate of the position of the phase equilibrium, which must be a monotonically increasing function at the interface of the two domains,[9] a straight line has been fitted through the five diamonds closest to the squares disregarding the diamonds at lower pressure (Figure 7):

I-III: $P = -439.3 + 2.483\ T$ (10)

with P in MPa and T in K.
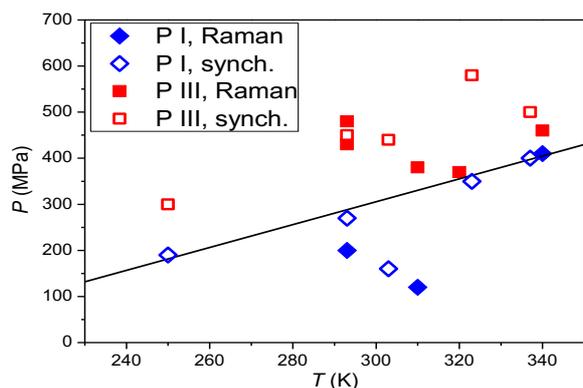
Figure 7. The observation of the appearance of form III with increasing pressure (squares) and the appearance of form I with decreasing pressure (diamonds) in synchrotron (open symbols) [29] and Raman measurements (filled symbols) (Figures 6 and S1-S6) at various temperatures (See also Table S2). Scatter is due to limited control over the pressure in the diamond anvil cell. The line is a linear fit to selected data (see text) and is an approximation of the I-III phase equilibrium.

Discussion

The relative stability ranking between the two-phase equilibria I-II and I-III

In Figures 8a and b, the phase diagrams are provided of the dimorphic systems I-II and I-III containing the phase equilibria between the solids, the liquid (L) and the vapour phase (V). These two phase diagrams have been published previously.[23,][29] They look alike in the sense that both are enantiotropic systems that become monotropic by increasing pressure. The main difference is that the transition temperatures of form III under ordinary conditions III-I(-V) and III-L(-V) are much lower in temperature than for form II. The coordinates belonging to the triple points in the two figures can be found in Table 3, which will be discussed in the last section. The only information missing in the present trimorphic system is the location of the II-III equilibrium curve, because it is exclusive to the unknown II-III phase diagram.

While combining the two dimorphic phase diagrams (Figure 8), it should not be forgotten that the stable and metastable

phase equilibria depicted in the two phase diagrams are relative to the phases within each phase diagram. Thus, the absolute stability ranking can change for phase equilibria and phases when phase diagrams are merged, but the relative stability ranking between phases remains the same. It can be seen that the I-III equilibrium is located in a domain, where form I is metastable, because it is already supposed to have transformed into form II, which stable I-II equilibrium occurs at a lower pressure. It implies that the I-III equilibrium is metastable.

This can also be judged from the melting equilibrium I-L. At 57 MPa this melting equilibrium becomes metastable while crossing the I-II-L triple point. Therefore when meeting the I-III-L triple point at 687 MPa, the I-L melting line will be metastable. It implies that the entire stability ranking around the triple point I-III-L decreases with one level rendering the I-III equilibrium metastable. The III-L melting equilibrium in between the metastable I-III and I-L equilibria has therefore become supermetastable.

Thus the I-II equilibrium is stable, whereas the I-III equilibrium is metastable at the positions in the phase diagram where they have been observed experimentally. This conclusion will be used in the next section to determine the global position of the intersection of the two equilibrium lines, the I-II-III triple point.

The positions of the II-III phase equilibrium and the triple point I-II-III based on thermodynamic arguments

Before placing the II-III phase equilibrium in the trimorphic phase diagram, its slope and the relative stabilities of the phases II and III at each side of the phase equilibrium will be determined. As mentioned in the introduction, the slopes of two-phase equilibria can be calculated with the Clapeyron equation (eq. 1), for which one needs the difference in entropy between the two phases and the difference in specific volume. In a previous publication,[23] it has been reported that the enthalpy change from form II into form I at the equilibrium temperature of 306 K equals $\Delta_{II \to I}h$ = 8.355 J g^{-1}.[23] This leads to an entropy difference between the two forms I and II of $\Delta_{II \to I}s$ = 0.0273 J g^{-1} K^{-1}. The I-III equilibrium line, eq. 10 has a slope of
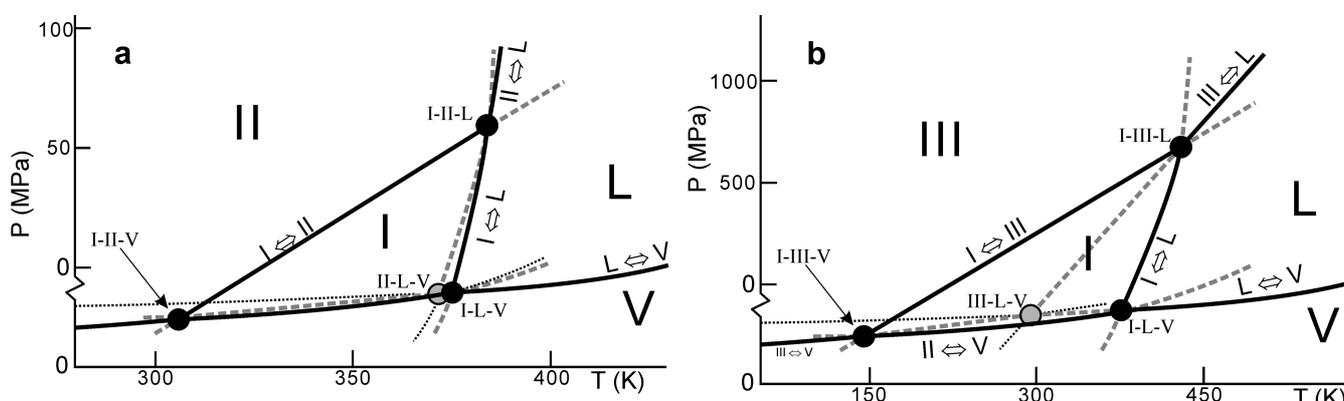
Figure 8. (a) Pressure-temperature phase diagram for the phases I, II, L (liquid), and V (vapour).[23] **(b)** Pressure-temperature phase diagram for the phases I, III, L, and V.[29] The solid lines are stable phase equilibria, the grey broken lines are metastable phase equilibria, and the black dotted lines are supermetastable phase equilibria. For clarity only the stable part of the sublimation curves (solid-vapour) has been drawn. Solid circles are stable triple points and the grey circle is a metastable triple point. Stable and metastable are defined in relation to the phases present in the diagram; therefore the stability degree is not necessarily final. Pressure and temperature are to scale, except for the pressure part of the vapour phase (the part between the two zero's on the pressure range)

ARTICLE

2.483 MPa K^{-1}. At 300 K, this equilibrium is located at 306 MPa. Inserting this pressure in the expressions 2 and 8, the volume for form I at 293 K is found to be 1110 Å^3 and that of form III is 1050 Å^3, leading to the difference $\Delta_{III\rightarrow I}V$ = +59.9 Å^3 and in terms of specific volume $\Delta_{III\rightarrow I}v$ = 0.0431 cm^3 g^{-1}. The volume difference multiplied by the slope (eq. 1) will lead to the entropy of transition, in this case $\Delta_{III\rightarrow I}s$ = 2.483 × 0.0431 = 0.1069 J g^{-1} K^{-1}. Using the two consecutive transitions III → I → II (please note the change in sign for the values of the I → II transition), which in terms of state functions is equivalent to III → II, the entropy of transition $\Delta_{III\rightarrow II}s$ = 0.1069 − 0.0273 = 0.0796 J g^{-1} K^{-1}.

The entropy increase going from form III to form II, indicates that form III contains less entropy than form II and in relation to the II-III equilibrium curve, form III will therefore be the more stable phase at low temperature and form II at high temperature relative to their equilibrium. In relation to the density, form II appears to have a slightly smaller specific volume (eq. 7 and 8). This implies that the change in volume on transition of form III into form II is a small, negative value. With the Clapeyron equation and the preceding values, the slope of the III-II equilibrium becomes negative and rather steep due to the small negative volume difference. For the sake of convenience the III-II equilibrium can be taken vertical with form III stable on the left at low temperature and form II stable on the right at high temperature (See Figure 9).

What is the location of the steep and negative III-II transition in the trimorphic phase diagram? Necessarily this equilibrium intersects the I-II-III triple point determined by the intersection of the two equilibrium lines I-II and I-III (Figure 9). In the case that this triple point can be found at low temperature (scenario 1 in Figure 9), the I-II equilibrium is more stable at pressures and temperatures above the I-II-III triple point. Once the I-II equilibrium intersects the triple point towards lower pressures and temperatures, it will decrease in stability ranking. The I-III equilibrium has a lower ranking and will
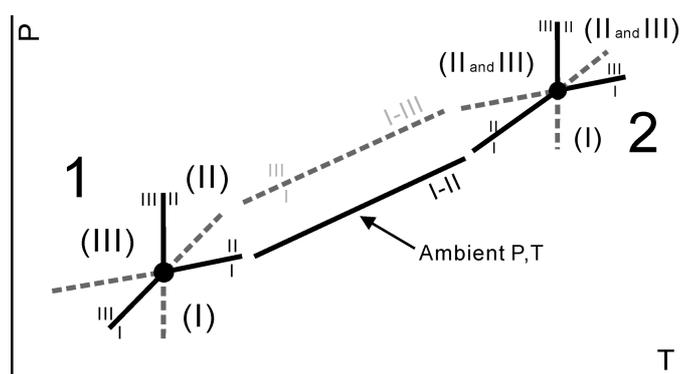
Figure 9. Two scenario's for the intersection of the I-II (stable: solid black line) and the I-III (metastable: grey broken line) equilibrium lines. Only one intersection, triple point I-II-III (solid black circle), can exist. Scenario 1 at low pressure and low temperature results in a thermodynamically consistent triple point with a stable domain for each of the solid phases (marked in parentheses). In scenario 2, the triple point at high temperature and high pressure, forms II and III have to be stable under the same conditions, which is thermodynamically impossible. Thus triple point I-II-III must for thermodynamic consistency be found below ambient pressure and temperature.

increase in ranking when intersecting the triple point. This leads to the relative stability ranking of the two-phase equilibria depicted in Figure 9, implying that the II-III equilibrium is more stable above the triple point than below in accordance with the alternation rule. It can be seen that scenario 1 is thermodynamically consistent as each phase possesses a stable phase region indicated in parentheses. It can also be seen that a limited change of the II-III equilibrium towards a more negative slope changes little in the overall position of the phase regions.

It can be shown that the alternation rule forbids the intersection of the equilibrium lines I-II and I-III at high pressure and temperature (Figure 9, scenario 2). In that case, the I-II equilibrium would be stable below the triple point as indicated in Figure 9. Furthermore, equilibrium I-III would be metastable below the triple point and become stable above the triple point. The alternation rule still requires that the III-II equilibrium is stable above triple point I-II-III. However, because the position of relative stability at each side of the three two-phase equilibria does not change, the configuration at a high pressure/temperature triple point leads to an inconsistent picture, in which a stable I-II equilibrium requires a stable form II at the upper left corner of the triple point (Figure 9, scenario 2), whereas the stable equilibrium II-III requires that form III is stable under the exact same conditions. A similar inconsistency occurs at the upper right corner of the triple point. This is thermodynamically impossible and thus the triple point I-II-III can only be located at low (or negative) pressure and low temperature in accordance with scenario 1.

The trimorphic pressure-temperature phase diagram obtained from observed data and direct inferences

The entire trimorphic phase diagram will be constructed step by step as illustrated in Figure 10. In Figure 10a the experimentally observed II-I transition[23] is placed in the pressure-temperature phase diagram following the expression (*P* in MPa and *T* in K):[23]

I-II: P = −224.6 + 0.7339 T (11)

In the same way, the melting equilibrium of form I, reported in the same paper, is defined by the following equation (*P* in MPa and *T* in K, R is the Pearson correlation coefficient):[23]

I-L: P = 16270 − 91.80 T + 0.1291 T^2 R^2 = 0.99   (12a)

This leads to the (partial) phase diagram representing phases I and II (Figure 10b). This (part of the) phase diagram is based on experimental data; the melting equilibrium of form I has been obtained by high-pressure measurements and the temperature of the solid-solid transition II-I, its enthalpy, and the volume differences between the two phases have been obtained by direct measurement.[23] The slope of the II-I equilibrium has been calculated with the Clapeyron equation with an error of about 8% leading to a straight equilibrium line

as solid-solid phase equilibria are straight over considerable pressure and temperature ranges.[21, 40-47]

Equation 12a, the melting equilibrium of form I, is problematic because the parabola is very suitable for interpolation; however, its curvature makes extrapolation for topological applications difficult. Because solid-liquid phase equilibria must be monotonically increasing functions,[9] a linear approximation of eq. 12a will be used, which has been obtained by fitting a linear expression to the data points obtained for the melting of form I. This has led to the following equation:

I-L (linear approx.): $P = -3375 + 8.96\ T$ $R^2 = 0.98$ (12b)

Using equations 11 and 12b, the coordinates of the triple point I-II-L become 383 K, 57 MPa (Figure 10b and Table 3).

Because the melting equilibrium of form I is stable, it follows that the melting equilibrium of form II lies in between the eqs. 11 and 12 and that it is metastable up to the triple point I-II-L above which it becomes the stable melting equilibrium (Figure 10c). The equilibria I-II and I-L become metastable above triple point I-II-L as indicated by the dashed lines in Figure 10b. Below the intersection with the temperature axis ($P = 0$ MPa), I-II and I-L also become metastable dashed lines as they meet the vapour phase (triple points I-II-V and I-L-V), which in Figure 10 has been set equal to the T-axis for simplicity.

There are several ways to obtain an expression for the II-L equilibrium, which evidently are all estimates. One approach is to calculate the melting temperature at ordinary pressure through the vapour pressure equilibrium lines expressed by the Clausius-Clapeyron equation. This approach has been described previously[23] and will not be repeated here; it leads to a melting point for form II of 372 K together with a vapour pressure of 45 Pa. It should not escape the reader that this is another triple point in the phase diagram, namely II-L-V (Table 3). Using the coordinates of the triple points I-II-L and II-L-V, the equilibrium line II-L can be defined by a linear expression:

II-L: $P = -1891 + 5.08\ T$ (13)

This fully defines the lines in Figure 10c, which is topologically equivalent to Figure 8a.

The two-phase equilibrium I-III was obtained through X-ray diffraction measurements in combination with the data obtained by the Raman measurements under pressure (see Figure 7 and 10d). This has led to a refined expression for the I-III equilibrium (eq. 10) in relation to the line reported previously.[29]

Since eq. 11 above describes the equilibrium between phases I and II, and eq. 10 the equilibrium between phases I and III, at the intersection, phases I, II, and III must be in equilibrium and this leads therefore to the coordinates of triple point I-II-III: $T = 123$ K and $P = -134$ MPa. These coordinates are consistent with the conclusion reached independently above and based on the alternation rule that the I-II-III triple point must be located at low temperature and low pressure (here negative pressure) in the phase diagram (Figure 10e).

It should be realized that tracing the equilibrium I-III to the I-II-III triple point, it intersects the solid-vapour equilibrium, which is the I-III-V triple point. Because the temperature is low, the pressure will be negligible and can be set to 0 MPa. In that case eq. 10 results in a temperature of 177 K for the I-III-V triple point. With this temperature and Clausius-Clapeyron data from a previous article[29], the vapour pressure can be calculated leading to 1.5×10^{-14} MPa or 1.5×10^{-8} Pa, thus indeed negligible ≈ 0 Pa. Because the I-III equilibrium enters the domain in which the vapour is the most stable phase, the stability hierarchy of the I-III equilibrium will decrease one level. This is indicated in Figure 10d by a change in the type of line from dashed to dotted, just as the other two-phase equilibria decrease one stability level.

Table 3. Triple point coordinates[a,b]

Phases	T (K)	P (Pa)	Ref
I-II-V	306	0.047	[23]
I-L-V	376	57	[23]
I-II-L	383	57×10^6	[23]
II-L-V	372	45	[23]
I-II-III	123	-134×10^6	This work
I-III-V	177	0	[29], this work
II-III-V	112	0	This work
II-III-L	185	-950×10^6	This work
I-III-L	453	687×10^6	[29], this work
III-L-V	341	6.6	[29], this work

[a] I: solid phase I, II: solid phase II, III: solid phase III, L: liquid, V: vapour phase, [b] see also the supplementary information

To place the II-III equilibrium in the phase diagram the triple point I-II-III will be used. An estimate of the slope of the equilibrium can be obtained with the Clapeyron equation.

The entropy difference was obtained in the previous section and was found to be $\Delta_{III \to II} s = 0.0796$ J g^{-1} K^{-1}. Strictly speaking, this entropy difference is valid at 300 K, where it has been determined, and going down in temperature, the entropy difference will most likely decrease as all absolute entropies decrease with decreasing temperature. Important to retain is however that the entropy change from form III to form II is positive.

The change in volume for the transition of III into II has not been measured either, as the transition has not been observed. However, going down in temperature, which will cause shrinking of the unit cells, can be considered equivalent to going up in pressure. At high pressure the volume difference between form II and form III is constant and taking the two expressions 7 and 8 at 1000 MPa for example leads to $\Delta_{III \to II} V = -8.45$ Å^3 or -0.0061 cm^3 g^{-1}. This volume difference must be close to the lower limit of the volume difference between the two solid forms II and III.

The slope that is obtained from the volume and entropy differences with eq. 1 equals dP/d$T = 0.0796/-0.0061 = -13.1$ MPa K^{-1}. As was stated above, the entropy may actually be smaller at lower temperatures, indicating that the absolute value of the slope will most likely be lower, however, the slope is necessarily negative, because the volume difference is negative. With the slope the following expression can be

obtained for the II-III equilibrium line (knowing that it should pass through the triple point I-II-III: 123 K, −134 MPa, see Figure 10f):

II-III: P = 1474 −13.1 T (14)

With this line, the position of two other triple points can be determined, that of II-III-V (Figure 10f), which is the intersection of II-III, II-V, and III-V, and that of II-III-L (Figure 10g), which is the intersection of II-III, II-L and III-L.

The triple point of II-III-V equals the intersection of the equilibrium II-III with the line P = 0, as the vapour pressure of the solids is again negligible. With eq. 14, the triple point is found at 112 K (see Table 3 and Figure 10f).

The triple point II-III-L is the result of an extended extrapolation and will always contain a large margin of error. It can be obtained from the intersection of the II-L equilibrium, which is known (eq. 13) and the II-III equilibrium (eq. 14, Figure 10g). This leads to a triple point at very large negative pressures, due to the steep slope of the II-III equilibrium: 185 K

and −950 MPa for triple point II-III-L.

As the equilibrium III-L also intersects the triple point II-III-L, this information can be used to place the last equilibrium curve III-L in the phase diagram. First, tracing the I-III equilibrium up to high positive pressures, it will intersect the I-L equilibrium leading to the triple point I-III-L (Figure 10g). Using eqs. 12b and 5, the coordinates for the I-III-L triple point are: T = 453 K and P = 687 MPa. This is the second point on the III-L equilibrium line. Tracing a straight line between the II-III-L and I-III-L triple points leads to the following expression for the III-L equilibrium (Figure 10h):

III-L: P = −2078 + 6.1 T (15)

Using eq. 15, the final triple point, III-L-V, in the phase diagram can be estimated by determining the temperature at which III-L intersects P = 0 (Figure 10h). It leads to a triple point temperature of 341K and using the expression of the vapour pressure of the liquid[23], it can be calculated that the actual pressure of the system would be 6.6 Pa (Through triple point
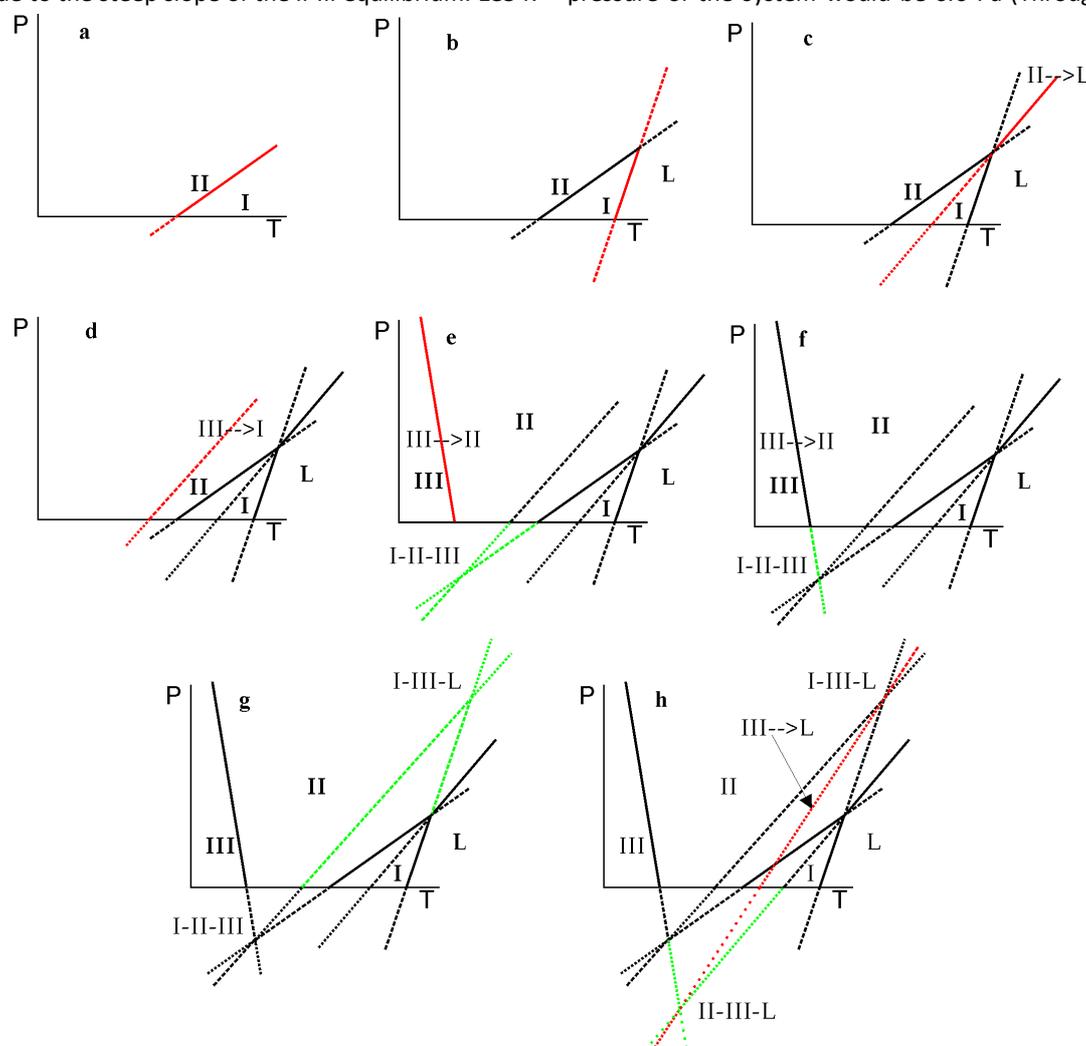
Figure 10. The step-by-step construction of the topological phase diagram of trimorphic L-tyrosine ethyl ester (see text); the red lines represent newly added equilibrium lines, the green lines are obtained by extrapolation; solid lines: stable equilibria, dashed lines: metastable equilibria, dotted lines: supermetastable equilibria, dotted lines with large spacing: super-supermetastable equilibria and three intersecting lines represent triple points. Pressure and temperature axes are not to scale.
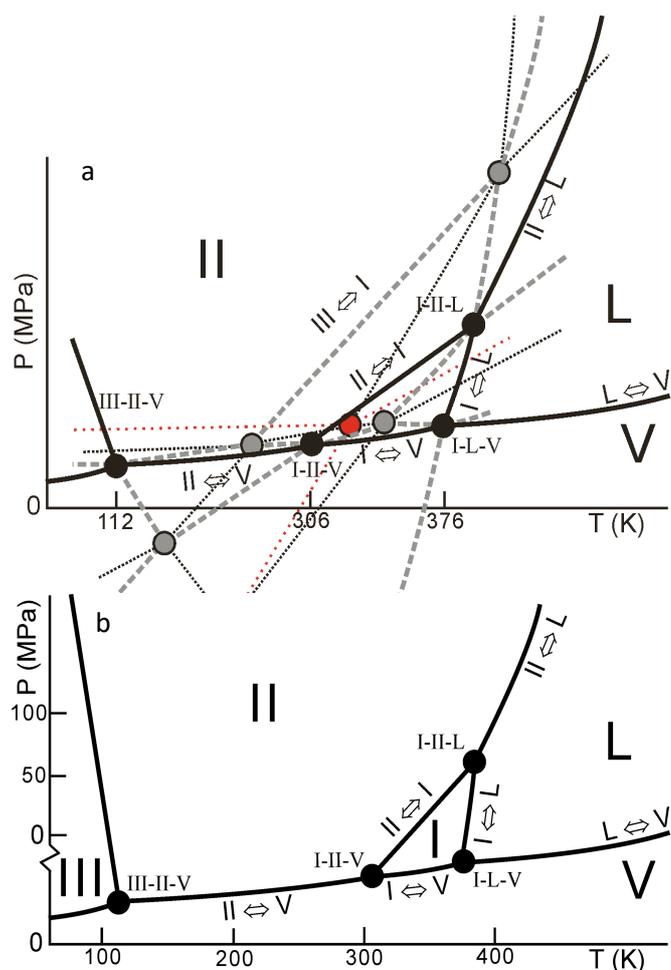
Figure 11. (a) The complete topological pressure-temperature phase diagram of the trimorphism of L-tyrosine ethyl ester (scales are not linear) **(b)** The stable phase diagram of L-tyrosine ethyl ester (linear scales except for the pressure of the vapour phase). Solid lines: stable two-phase equilibria, grey dashed lines: metastable two-phase equilibria, dotted lines: supermetastable two-phase equilibria, dotted lines with large spacing (red): super-super metastable two-phase equilibria. Black solid circles: stable triple points, grey circles metastable triple points, red circles: supermetastable triple points.

III-L-V, an expression for the vapour pressure of solid form III can be obtained, see eq. SI.15 in the supplementary information).

Even if the margins of error of the last four points in Table 3 are quite large, the overall layout of the 10 triple points defines the basic phase behaviour in the system, which includes stable phase regions for all three solid forms, a stable melting equilibrium for form I at low pressure and a stable melting equilibrium for form II at high pressure. Form III does not have a stable melting equilibrium, because the slope of III-L is slightly steeper than that of II-l, so with increasing pressure these two equilibria diverge.

Conclusions

In figure 11a, the complete topological pressure-temperature phase diagram is presented that has been constructed step-by-

step in Figure 10. With the available experimental data[23,24,29] and thermodynamic constraints, it has been deduced that form III has a stable pressure-temperature domain at very low temperature. This result has been obtained without explicitly calculating the Gibbs free energy; however by using the Clapeyron equation and the alternation rule, the phase diagram –the projection of the intersections of the Gibbs free energy surfaces on the pressure-temperature plane- can be obtained. The result depicted in Figure 11a can be reduced to the stable phase diagram, which is provided in Figure 11b.

The data to construct this phase diagram are the volume data from X-ray diffraction under ordinary pressure conditions for forms I and II[23] and under pressure for forms I, II, and III in addition to the observation of the II-I and I-L transitions by DSC under ordinary pressure conditions[23] and the I-L melting equilibrium by DTA under high-pressure conditions[23]. Furthermore, the I-III equilibrium line was obtained through X-ray[29] and Raman data under pressure for different temperatures.

Thermodynamic arguments placed the I-II-III equilibrium at low pressure (negative pressure in this case) and low temperature while implying that the II-III equilibrium possesses a rather steep slope. The triple point position was independently confirmed by extrapolation of the two equilibrium lines I-II and I-III. Once the I-II, I-III, II-III, and the I-L phase equilibria were located, the rest of the phase diagram could be deduced through the triple points and the alternation rule.

The phase diagram as presented in this paper is valid in relation to the three known solid phases of L-tyrosine ethyl ester. More high-quality data will improve the accuracy of the positions of the two-phase equilibrium lines, I-III and II-III in particular, and of the triple point coordinates, I-II-III in particular. Moreover, it is always possible that a new solid form is discovered at a later stage. It will not invalidate the phase diagram published here; it will simply change the ranking of certain phase equilibria relative to the new phase.

As mentioned in the introduction, in addition to the phase diagram, the kinetic behaviour of the system is important. In the present case, form II transforms into form I on heating under ordinary conditions, however, form I has not been observed to revert back to form II. Although, this has been discussed in a previous article,[23] it should be mentioned here that the determination of the solid-solid transition of form II into form I has not been straightforward. DSC measurements, in fact, tend to overshoot solid-solid equilibria and at a 10 K min^{-1} heating rate the transition occurs around 65°C. Only by using a series of different heating rates, can it be shown that the real equilibrium temperature from form II into form I is found at 33 °C, which has subsequently been confirmed by X-ray diffraction.

Form I readily transforms into form III on increasing pressure at high temperatures and form III transforms readily back into form I at high temperatures on releasing the pressure. Below ambient temperature, this transition rate rapidly declines and it becomes much harder to observe a clear transition between forms I and III. The fact that form II does not appear under pressure either from form I or from form III is caused by the

necessary conformational change as mentioned in the introduction between form II and the two forms I and III. The limited volume available under pressure effectively decreases the transformation kinetics rapidly to zero similar to the lack of conversion between two polymorphs of tolazamide.[48] Nonetheless, one would expect form II to crystallize under pressure if forms I or III could be dissolved as in the case of 4,4'-bipyridinium.[49]

Finally, are measurements under pressure necessary to construct this type of phase diagrams? For known polymorphs, this is not necessarily the case, as other examples attest that have been obtained with data based only on DSC and "ordinary" pressure X-ray data.[17, 50-52] However, it is obvious in the present case that without pressure L-TEE polymorph III would never have been observed. In addition, the high-pressure experiments have helped to position the phase equilibria more accurately in relation to the temperature and pressure conditions. Thus in the end, the answer to the question of whether to carry out measurements under pressure simply depends on how precisely one needs to understand the phase behaviour of the system.

Conflicts of interest

There are no conflicts to declare.

Acknowledgements

Notes and references

1. J. Bernstein, *Polymorphism in Molecular Crystals*, Oxford University Press, Oxford (UK), 2002.
2. G. M. Day, W. D. S. Motherwell and W. Jones, *Phys. Chem. Chem. Phys.*, 2007, **9**, 1693-1704.
3. M. A. Neumann, J. van de Streek, F. P. A. Fabbiani, P. Hidber and O. Grassmann, *Nat. Commun.*, 2015, **6**, 7793-7799.
4. A. M. Reilly, R. I. Cooper, C. S. Adjiman, S. Bhattacharya, A. D. Boese, J. G. Brandenburg, P. J. Bygrave, R. Bylsma, J. E. Campbell, R. Car, D. H. Case, R. Chadha, J. C. Cole, K. Cosburn, H. M. Cuppen, F. Curtis, G. M. Day, R. A. DiStasio Jr, A. Dzyabchenko, B. P. van Eijck, D. M. Elking, J. A. van den Ende, J. C. Facelli, M. B. Ferraro, L. Fusti-Molnar, C.-A. Gatsiou, T. S. Gee, R. de Gelder, L. M. Ghiringhelli, H. Goto, S. Grimme, R. Guo, D. W. M. Hofmann, J. Hoja, R. K. Hylton, L. Iuzzolino, W. Jankiewicz, D. T. de Jong, J. Kendrick, N. J. J. de Klerk, H.-Y. Ko, L. N. Kuleshova, X. Li, S. Lohani, F. J. J. Leusen, A. M. Lund, J. Lv, Y. Ma, N. Marom, A. E. Masunov, P. McCabe, D. P. McMahon, H. Meekes, M. P. Metz, A. J. Misquitta, S. Mohamed, B. Monserrat, R. J. Needs, M. A. Neumann, J. Nyman, S. Obata, H. Oberhofer, A. R. Oganov, A. M. Orendt, G. I. Pagola, C. C. Pantelides, C. J. Pickard, R. Podeszwa, L. S. Price, S. L. Price, A. Pulido, M. G. Read, K. Reuter, E. Schneider, C. Schober, G. P. Shields, P. Singh, I. J. Sugden, K. Szalewicz, C. R. Taylor, A. Tkatchenko, M. E. Tuckerman, F. Vacarro, M. Vasileiadis, A. Vazquez-Mayagoitia, L. Vogt, Y. Wang, R. E. Watson, G. A. de Wijs, J. Yang, Q. Zhu and C. R. Groom, *Acta Crystallogr. B*, 2016, **72**, 439-459.
5. J. Bernstein and A. T. Hagler, *J. Am. Chem. Soc.*, 1978, **100**, 673-681.
6. A. T. Hagler and J. Bernstein, *J. Am. Chem. Soc.*, 1978, **100**, 6349-6354.
7. J. D. Dunitz and J. Bernstein, *Acc. Chem. Res.*, 1995, **28**, 193-200.
8. S. L. Price, *Phys. Chem. Chem. Phys.*, 2008, **10**, 1996-2009.
9. R. Ceolin and I. B. Rietveld, *Eur. Phys. J. - S.T.*, 2017, **226**, 1001-1015.
10. M. Zilka, D. V. Dudenko, C. E. Hughes, P. A. Williams, S. Sturniolo, W. T. Franks, C. J. Pickard, J. R. Yates, K. D. M. Harris and S. P. Brown, *Phys. Chem. Chem. Phys.*, 2017, **19**, 25949-25960.
11. R. D. L. Johnstone, A. R. Lennie, S. F. Parker, S. Parsons, E. Pidcock, P. R. Richardson, J. E. Warren and P. A. Wood, *CrystEngComm*, 2010, **12**, 1065-1078.
12. M. Bujak, D. Blaser, A. Katrusiak and R. Boese, *Chem. Commun.*, 2011, **47**, 8769-8771.
13. A. Gavezzotti, *Cryst. Res. Technol.*, 2013, **48**, 793-810.
14. J. Nyman and G. M. Day, *Phys. Chem. Chem. Phys.*, 2016, **18**, 31132-31143.
15. M. Barrio, E. Maccaroni, I. B. Rietveld, L. Malpezzi, N. Masciocchi, R. Céolin and J.-L. Tamarit, *J. Pharm. Sci.*, 2012, **101**, 1073-1078.
16. J. Bauer, S. Spanton, R. Henry, J. Quick, W. Dziki, W. Porter and J. Morris, *Pharm. Res.*, 2001, **18**, 859-866.
17. R. Céolin and I. B. Rietveld, *Ann. Pharm. Fr.*, 2015, **73**, 22-30.
18. R. A. E. Castro, T. M. R. Maria, A. O. L. Evora, J. C. Feiteira, M. R. Silva, A. M. Beja, J. Canotilho and M. E. S. Eusebio, *Cryst. Growth Des.*, 2010, **10**, 274-282.
19. R. Céolin, V. Agafonov, D. Louër, V. A. Dzyabchenko, S. Toscani and J. M. Cense, *J. Solid State Chem.*, 1996, **122**, 186-194.
20. S. Toscani, R. Céolin, L. Ter Minassian, M. Barrio, N. Veglio, J.-L. Tamarit, D. Louër and I. B. Rietveld, *Int. J. Pharm.*, 2016, **497**, 96-105.
21. R. Ceolin, S. Toscani, I. B. Rietveld, M. Barrio and J.-L. Tamarit, *Eur. Phys. J. - S.T.*, 2017, **226**, 1031-1040.
22. I. Gana, M. Barrio, C. Ghaddar, B. Nicolai, B. Do, J. L. Tamarit, F. Safta and I. B. Rietveld, *Mol. Pharmaceut.*, 2015, **12**, 2276-2288.
23. I. B. Rietveld, M. Barrio, J.-L. Tamarit, B. Nicolaï, J. Van de Streek, N. Mahé, R. Céolin and B. Do, *J. Pharm. Sci.*, 2011, **100**, 4774-4782.
24. B. Nicolaï, N. Mahé, R. Céolin, I. B. Rietveld, M. Barrio and J.-L. Tamarit, *Struct. Chem.*, 2011, **22**, 649-659.
25. A. H. Kahns, A. Buur and H. Bundgaard, *Pharm. Res.*, 1993, **10**, 68-74.
26. C. H. Huang, R. Kimura, R. Bawarshinassar and A. Hussain, *J. Pharm. Sci.*, 1985, **74**, 1298-1301.
27. C. E. McDonald and A. K. Balls, *J. Biol. Chem.*, 1956, **221**, 993-1003.
28. A. N. Glazer, *J. Biol. Chem.*, 1966, **241**, 635-&.
29. B. Nicolaï, J.-P. Itié, M. Barrio, J. L. Tamarit and I. B. Rietveld, *CrystEngComm*, 2015, **17**, 3974-3984.
30. A. F. Pieret, F. Durant, M. Griffé, G. Germain and T. Debaerdemaeker, *Acta Crystallogr. Sect. B: Struct. Sci.*, 1970, **26**, 2117-2123.
31. A. J. Cruz-Cabeza and J. Bernstein, *Chem. Rev.*, 2014, **114**, 2170-2191.
32. M. Jenau, J. Reuter, J. L. Tamarit and A. Wurflinger, *J. Chem. Soc. Faraday Trans.*, 1996, **92**, 1899-1904.
33. J. C. Chervin, B. Canny, J. M. Besson and P. Pruzan, *Rev. Sci. Instrum.*, 1995, **66**, 2595-2598.
34. A. Hammersley, *Fit2D v12.077 (Computer Software)*, 1987-2005, http://www.esrf.eu/computing/scientific/FIT2D/fit2d_abstract.html.

35. A. A. Coelho, *TOPAS Academic version 4.1 (Computer software)*, 2007.

36. A. A. Coelho, *J. Appl. Crystallogr.*, 2003, **36**, 86-95.

37. R.J. Angel, J. Gonzalez-Platas, M. Alvaro, *Z. Kristallogr.*, 2014, **229**(5), 405-419.

38. R.J. Angel, M. Mazzucchelli, M. Alvaro, P. Nimis, F. Nestola, *Am. Mineral.*, 2014, **99**, 2146-2149.

39. C. Cappuccino, P. P. Mazzeo, T. Salzillo, E. Venuti, A. Giunchi, R. G. Della Valle, A. Brillante, C. Bettini, M. Melucci and L. Maini, *Phys. Chem. Chem. Phys.*, 2018, doi: 10.1039/c1037cp06679a.

40. I. Gana, M. Barrio, B. Do, J.-L. Tamarit, R. Céolin and I. B. Rietveld, *Int. J. Pharm.*, 2013, **456**, 480-488.

41. P. Negrier, M. Barrio, J. L. Tamarit and D. Mondieig, *J. Phys. Chem. B*, 2014, **118**, 9595-9603.

42. B. B. Hassine, P. Negrier, M. Barrio, D. Mondieig, S. Massip and J. L. Tamarit, *Cryst. Growth Des.*, 2015, **15**, 4149-4155.

43. P. Negrier, M. Barrio, M. Romanini, J. L. Tamarit, D. Mondieig, A. I. Krivchikov, L. Kepinski, A. Jezowski and D. Szewczyk, *Cryst. Growth Des.*, 2014, **14**, 2626-2632.

44. J. L. Tamarit, M. Barrio, L. C. Pardo, P. Negrier and D. Mondieig, *J. Phys.: Condens. Matter*, 2008, **20**, 244110.

45. P. Negrier, M. Barrio, J. L. Tamarit, N. Veglio and D. Mondieig, *Cryst. Growth Des.*, 2010, **10**, 2793-2800.

46. B. Parat, L. C. Pardo, M. Barrio, J. L. Tamarit, P. Negrier, J. Salud, D. O. López and D. Mondieig, *Chem. Mater.*, 2005, **17**, 3359-3365.

47. M. Barrio, J. L. Tamarit, P. Negrier, L. C. Pardo, N. Veglio and D. Mondieig, *New J. Chem.*, 2008, **32**, 232-239.

48. A. Y. Fedorov, D. A. Rychkov, E. A. Losev, B. A. Zakharov, J. Stare and E. V. Boldyreva, *CrystEngComm*, 2017, **19**, 2243-2252.

49. M. Aniola and A. Katrusiak, *Cryst. Growth Des.*, 2015, **15**, 764-770.

50. I. B. Rietveld and R. Céolin, *J. Therm. Anal. Calorim.*, 2015, **120**, 1079-1087.

51. I. B. Rietveld and R. Céolin, *J. Pharm. Sci.*, 2015, **104**, 4117-4122.

52. R. Céolin and I. B. Rietveld, *Ann. Pharm. Fr.*, 2017, **75**, 89-94.